J.Serb.Chem.Soc. 68(8–9)615–628(2003)
JSCS – 3070

UDC 531.61.094.4:541.144:531.3
Original scientific paper

Energy storage in the photosynthetic electron-transport chain. An analogy with Michaelis-Menten kinetics

DEJAN MARKOVIĆ

Faculty of Technology, 16000 Leskovac, Serbia and Montenegro (E-mail: dzmarkovic@ptt.yu)

(Received 28 August 2002)

Abstract: Simultaneous measurements of fluorescence and thermal emission have been performed by applying combined fluorescence and photoacoustic techniques on isolated thylakoids pretreated by prolonged illumination with saturating light. The traces were used to create Lineweaver-Burk type plots, proving clearly at least a formal analogy between the kinetics of the mechanisms governing fluorescence and thermal emission from isolated thylakoids and Michaelis-Menten kinetics of enzymatic reactions. Two characteristic parameters were calculated from them (energy storage and half-saturation light intensity) in order to obtain a basic, initial response of the photosynthetic apparatus functioning under photoinhibition stress.

Keywods: photosynthetic electron-transport, reaction centers, energy storage, fluorescence, thermal emission.

INTRODUCTION

As the most fundamental life process on earth, photosynthesis is the focus of a vast body of research, spanning studies of femtosecond reactions at the molecular level through field studies requiring a whole season of observation. Photosynthesis takes place in chloroplasts thylakoids membranes. In all oxygen-evolving organisms, photosynthesis involves the co-operation of two pigment-protein complexes, known as photosystems I and II (PSI and PSII). They function in series in the so-called non-cyclic electron transport chain (ETC) to oxidize water, reduce $NADP^+$ and generate ATP. PSI can also function independently in a cyclic electron transport pathway to generate ATP.[1] It is widely accepted that PSII and PSI function according to the "Z-scheme" by which electrons released from water pass through PSII and on to PSI, generating the strong reductant necessary for $NADP^+$ reduction.[2,3] The cross section of a thylakoid membrane (with two two-photosystems) showing the direction of photosynthetic electron transport (PET) is shown in Fig. 1.[3] The two "energetic monettes" (NADPH and ATP), synthesized during the photosynthesis "light phase", provide the necessary energetic input for the "dark phase", consisting of cycles of biochemical reactions, and finishing with the final production of organic sugars.[4]

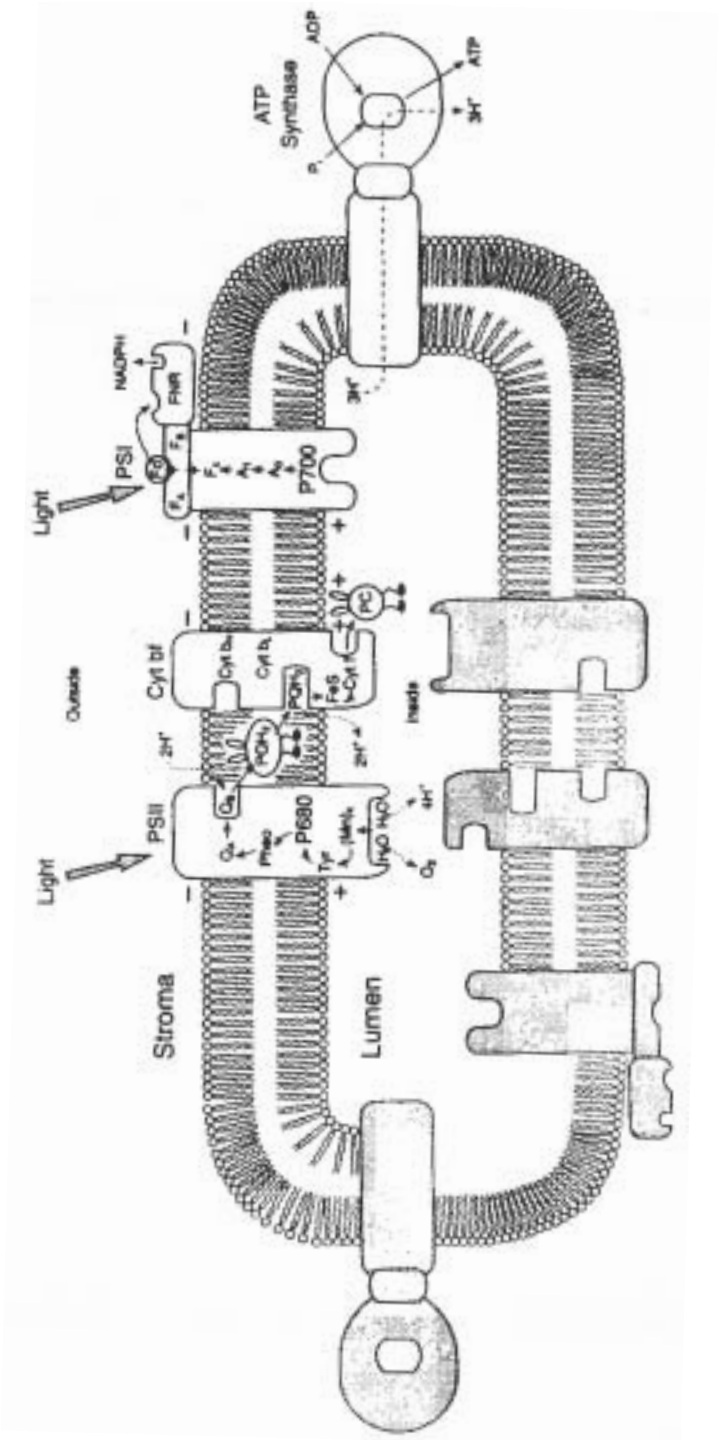
ATP Synthase
ADP
ATP
3H+
NADPH
FNR
PSI
P700
Light
Cyt bf
Outside
Inside
2H+
PSII
P680
Light
Stroma
Lumen
4H+

Fig. 1. Four major protein complexes are used for the production of the reducing power NADPH and ATP, both needed for the fixation of CO_2 and the production of glucose. *Photosystem II* (PSII, which oxidizes water to oxygen, reduces a plastoquinone molecule, and releases protons in the interior of the thylakoid membrane; it is also called water- plastoquinone oxido-reductase); *cytochrome b/f* (Cyt bf) complex (which oxidizes reduced plastoquinone, reduces a copper protein plastocyanin (PC), and releases protons in the interior of the thylakoid membrane; it is also called plastoquinol-plastocyanin oxido-reductase); *photosystem I* (PSI, which oxidizes reduced plastocyanin and reduces $NADP^+$,nicotinamide adenine dinucleotide phosphate, to NADPH; it is also called plastocyanin-ferredoxin oxido-reductase); and *ATP synthase* (which uses the membrane potential and proton gradient to produce ATP from ADP and inorganic phosphate). The electron transport is produced during the powering of the photosynthetic apparatus by simultaneous light absorption in both PSII and PSI, leading to electron transfer from the inner side of the thylakoid membrane to the outer side. *The other abbreviations*: Tyr – tyrosin, an amino acid on D_1 protein; $(Mn)_4$ – manganese cluster, having a still unresolved role in water decomposition; P680 and P700 – Chla molecules with absorption maximums at 680 and 700 nm, respectively, known as reaction traps for the reaction centers (RCs) of the PSII and PSI, respectively; Pheo – Pheophytin; Q_A and Q_B, one-electron and two-electron acceptors of PSII, also known as the "attached quinones" (to plastoquinone); PQH_2 – reduced plastoquinone; Cyt bL and Cyt bH – two different forms of Cyt b; FeS – Iron-sulfur proteins, donor and acceptor sides of PSI RC; Cyt f – cytochrome f; PC – Plastocyanin; A_o – Chla molecule with a special function; A_1 – Phylloquinone; F_X, F_A and F_B – different forms of the Fe–S centers; F_d – ferredoxin; FNR – ferredoxin/$NADP^+$ oxido-reductase; LHC-I – light harvesting pigment-protein complex of PSI (the same for PSII – not shown); P_i – inorganic phosphates. The mobile carriers, PQH_2 and PC have "the legs". *From*: Govindjee, "Milestones in photosynthesis research", *Probing Photosynthesis. Mechanisms, Regulation and Adaptation*, Taylor and Francis, 2000, p. 17.

Isolated thylakoid membranes may be considered as photocatalysts for water decomposition in the presence of visible light.[5] A manganese cluster plays a crucial role in the oxygen-evolving complex (OEC), in which a cycle-of-four oscillation (with the participation of a tyrosine residue) leads to the release of four protons, four electrons and the evolution of one O_2 molecule (at the lumenal side), all coming from two H_2O molecules[6] – see Eq. (1).

The incident light absorbed by antennas of light-harvesting chlorophyll-protein (LHCP) complexes is used in two different ways: to drive photosynthesis upon charge separation in the reaction center complexes (RCs) of photosystems I and II, or it is dissipated in the form of fluorescence or thermal emission. The fluorescence trace is characterized by a non-variable component (F_o) that does not depend on photochemistry and a variable part (F_v) which is highly dependent on the photochemical activity of PSII.[7] Thermal emission can be measured by photoacoustic spectroscopy (PAS), in which the released heat generates a pressure wave, detected by a sensitive microphone. The portion of incident light energy stored during the primary photochemical event (charge separation) in the electron-transport chain intermediates, defined as energy storage yield, can be estimated by comparing an (photochemically) active sample with an inactive one.[8]

Energy storage has been detected by PAS techniques in various entities: isolated thylakoids,[9,10] PSII particles,[11] algae[12–14] and leaves.[15–20] Although it has not been clarified yet, the origin of the energy storage was mostly attributed to PSII activity. In the absence of artificial electron acceptors, photoreduction of the plastoquinone (PQ) pool is believed to be a predominant reaction for energy storage in PSII and in cyclic PSI.[21,22] On the

other hand, variable fluorescence (F_v), and maximal fluorescence (F_m) indicate the partial and total closure of the PSII reaction centers, respectively, as a result of the reduction of quinones at the PSII acceptor side.

The relationship between Chl fluorescence and PAS signals has been studied in radish seedlings and in spinach leaves,[23–25] as well as in isolated thylakoids[26] and PSII particles.[27] It was found that energy storage was strongly correlated with the F_v,[28] expressed *via* photochemical fluorescence quenching, $qPF = (F_m - F_v)/F_m$, and *via* its thermal emission counterpart, photochemical heat quenching $qPH = (H_m - H_v)/H_m$. The evidence lies in the very similar dependence of *qPF&qPH* on the intensity (*I*) of the photoacoustic modulated measuring (PAS) beam; a couple of parameters with significant photosynthetic relevance can be extracted from it.[26,27] Such parameters can then be used to study the influence of some external factors with environmental aspects, such as temperature and photoinhibition. The latter, occuring "when plants are exposed to irradiation higher than it can convert or dissipate without harm",[29] is partly touched upon in this report.

EXPERIMENTAL

Thylakoids isolation

Thylakoids membranes were isolated from spinach leaves by grinding them in a Waring blender in the following buffer: 330 mM sorbitol, 20 mM *N*-tris(hydroxymethyl)methylglycine (Tricine) (pH 7.8), 10 mM NaCl, cooled to 0 ºC. The homogenate was then filtered through 2 layers of Miracloth and centrifuged at 3000 × g for 2 min at 4 ºC. The pellet was washed once with 50 mM Tricine (pH 7.8), 10 mM NaCl, and 5 mM $MgCl_2$, and then resuspended in 20 mM 2-(*N*-morpholino)ethanesulfonic acid (Mes)-NaOH (pH 6.0), 330 mM sorbitol, 2 mM $MgCl_2$, 1 mM NaCl, and 1 mM NH_4Cl at a chlorophyll concentration of 2 mg/cm^3, which was adjusted spectrophotometrically.

Fluorescence and photoacoustic measurements

For the simultaneous fluorescence and photoacoustic measurements (FL&PAS), thylakoid membranes were diluted to 250 μg/ml in their respective resuspension buffer and 1 cm^3 of the preparation was aspirated onto a nitrocellulose filter (Millipore, 0.4 μm pore size) using a gentle vacuum. The filter was cut to the proper dimensions for introduction into the photoacoustic cell. The measurements were made with a laboratory-constructed instrument using a MTEC photoacoustic cell in combination with a PAM-101 chlorophyll fluorometer (Walz, Effeltrich, FRG). The experiments were performed with 4 pulses over a 1278 s time scale with the following working parameters: first F_o = 5 s; 1st pulse delay = 5 s; pulse width = 2 s; 2nd pulse delay = 120 s; time between the pulses = 540 s; last photoacoustic time = 20 s; last F_o = 40 s (see Fig. 2). The light intensity (*I*) range of the modulated photoacoustic measuring (PAS) beam were: 1.24 (1st one), 1.36, 1.76, 2.4, 3.04 and 3.84 W/m^2 (the last one). Two excitation wavelengths of the PAS beam (λ_{PAS}) were employed: 680 and 700 nm.

The PAS beam (35 Hz) produces variable fluorescence (F_v) and thermal emission (H_v). A strong non-modulated background illumination from a quartz-halogen source (more than 150 W/m^2) was used to transiently close the PSII reaction centers, providing maximal fluorescence and thermal emission (F_m and H_m, respectively). The fluorescence initial level (F_o) was excited by using a 1.6 kHz fluorimeter modulated beam.

Photoinhibition treatment

Defrosted thylakoids (in the bulk) were thermostated at 21 ºC, prior to the photoinhibition experiment.

The photoinhibition experiment was performed with defrosted, thermostated thylakoids in the bulk, before the preparation of the filtered samples (and so, before the FL&PAS combined experiment, as well). The source of photoinhibition was the strong, saturating white light from a "Fiber Lite" lamp, model 170 D. The

saturation light from an optic fiber connected to the lamp was directed to the center of the cuvette containing the thylakoids bulk solution. The bulk solution was stirred with a magnetic stirrer, thus equalizing the average amount of light that the thylakoids absorb during light saturation. The bulk solutions were light-saturated for a few periods of time ($t_{ph.}$): 15, 30, 45, 60 and 100 min. A fresh bulk solution was always employed for a new photoinhibition time. At the end of the photoinhibition experiment (for the given time period), the bulk solution was kept in the dark and on ice. When required, 1 cm^3 aliquots of the bulk solution were taken, the filtered thylakoids were prepared in described manner, and then used for the combined FL&PAS experiment.

RESULTS

Typical simultaneous FL&PAS traces obtained from isolated thylakoids are shown in Fig. 2. The weak 1.6 kHz fluorometer excitation beam yielded the initial fluorescence (F_o), indicating that all reaction centers (RCs) were in the open state. The counterpart, H_o, was

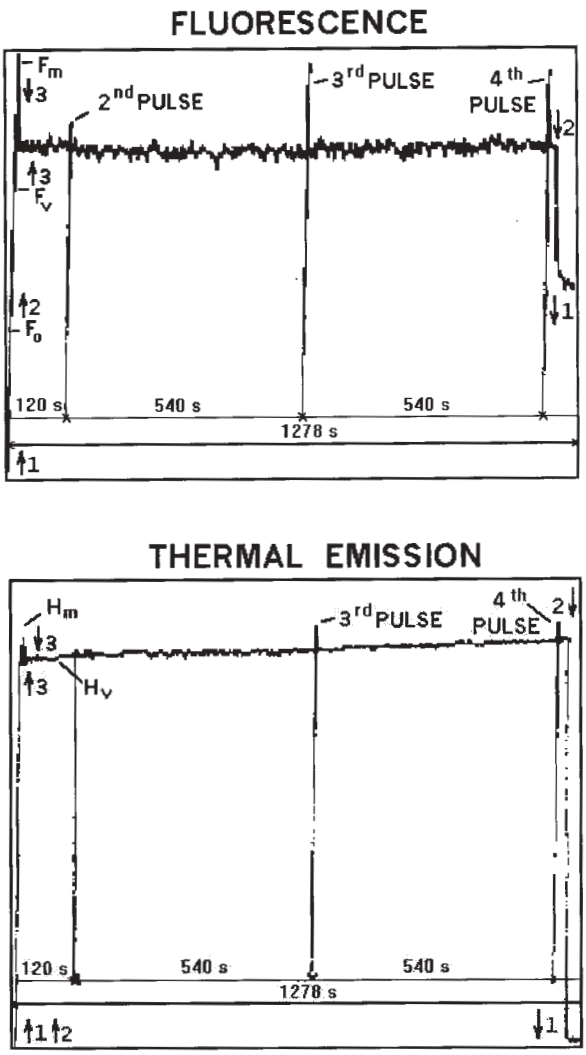

Fig. 2. Record from the simultaneous measurements of fluorescence (upper trace) and thermal emission (lower trace) in isolated and photoinhibited thylakoids. The numbers adjacent to arrows indicate: *1* – fluorescence probe beam; *2* – photoacoustic modulated measuring (PAS) beam (680 nm, 3.84 W/m^2, 35 Hz); *3* – saturated non-modulated background illumination. The other wavelength of the PAS beam (700 nm) as well as the other intensities produce very similar traces. The pulses width was 2 s, the distance between the 1st and 2nd pulse was 120 s, between the 2nd and 3rd and the 3rd and 4th 540 s. For some reason, the 2nd pulse on the thermal emission trace is hardly seen and is so unusable for calculations. The final buffer suspension with isolated thylakoids (the bulk solution) contained 250 μg/ml. F_o – the initial fluorescence level, induced by the fluorescence probe beam; F_v, H_v – variable fluorescence and thermal emission level, respectively, induced by the PAS beam; F_m, H_m – maximal fluorescence and thermal emission level, induced by saturating, non-modulated light.

not directly detectable.[21,28] The modulated PAS beam caused the fluorescence emission to rise from F_o to a variable F_v level. Simultaneously, a corresponding equivalent variable level of thermal emission (H_v) was achieved.

Subsequent addition of saturating pulses of non-modulated light induced maximal levels of fluorescence (F_m) and thermal emission (H_m). Unlike the F_v level, which reflects partial closure of the PSII reaction centers, F_m marks their total closure due to complete reduction of the plastoquinone pool and saturation of the electron transport.[7]

A ratio F_v/F_m, and *qPF*, photochemical fluorescence quenching, defined as $(F_m - F_v)/F_m$, may then serve as a measure of the RCs openness or closure[30,31] (the nomenclature used in this paper does not follow strictly the van Cooten and Snel recommendation[32] in a formal sense, but it has the same basic meaning). On the other hand, H_m is related to the state where no energy is stored. The energy storage yield, defined *via* photochemical heat quenching, $qPH = (H_m - H_v)/H_m$, represents the amount of absorbed energy, stored in the ETC redox intermediates, and therefore not released as heat during the modulation period of the PAS beam.[8]

All calculations were based on the 4 pulses in the case of *qPF* data (Fig. 2, upper trace), and on the 3 pulses in the case of *qPH* data (Fig. 2, lower trace). The 2nd pulse was almost absent in the thermal emission trace, or was of very irregular shape, unsuitable for calculation. Generally, the thermal emission trace was always weaker than its fluorescence counterpart. The values of *qPF* and *qPH* were calculated for the same numbered pulse; then, they were averaged since the particular *qPF&qPH vs. I* plots almost overlapped, on the same time scale. A clear correlation between *qPF* and *qPH* was seen from the shapes of the corresponding *qPF&qPH vs. I* plots, for both λ_{PAS} values (680 and 700 nm), and for different photoinhibition times (as in the absence of any photoinhibition - see previous reports [26,27]). At least in the case of fluorescence, the decline of *qPF* with increasing PAS beam intensities (*I*) was expected from the progressive closure of the RCs, as both photosystems are exposed to higher light intensities.

A mathematical model describing the kinetic behaviour of the photosynthetic electron transport chain, originally derived by Howel and Vieth,[5] was based on a few very defined assumptions:

(a) A thylakoid membrane can be considered as a microheterogeneous photocatalyst (permitting the decomposition of water under visible light), consisting of a collection of identical PET chains.

(b) The PET chains function independently of one another.

(c) There are two reaction centers (RCs) per one PET chain, one belonging to PSII (excited by λ = 680 nm), and the other belonging to PSI (excited by λ = 700 nm).

(d) The absorbed photons are equally distributed between the two reaction centers; the net excitation rates of the two reaction centers are equal and can be represented by a single photophysical process ($P + h\nu \rightarrow P^*$)

(e) The electron-transport rate is independent of the concentration of the terminal electron acceptor.

Bearing these assumptions in mind, water photocatalysis by thylakoid membranes may be presented by the following scheme.[5]

$$\begin{array}{c} 2\,H_2O + P^* \xrightarrow{k_D} P + O_2 + 4H^+ + 4e^- \\ k_d \downarrow\uparrow k_e I \\ P + h\nu \end{array} \qquad (1)$$

where P and P^* represent the concentrations of the RCs in the ground state and excited state, respectively; k_e is the rate constant for the excitation of RCs, and k_d is the rate constant for P^* deactivation, I represents the excitation intensity, and k_D is the overall photochemical rate constant, *i.e.*, the overal rate constant for all PET-related processes and reactions, permitted by the absorbed sunlight and leading to O_2 evolution.*

The net rate of P^* formation is:

$$dP^*/dt = k_e IP - k_d P^* - k_D P^* \qquad (2)$$

Within a very short time after illumination, a steady-state concentration of the excited reaction centers (P^*) is established. Setting the net rate equal to zero ($dP^*/dt = 0$) and solving for P^*:

$$P^* = k_e IP / (k_d + k_D) \qquad (3)$$

Introducing the following stoichiometric invariance:

$$P_o = P + P^* \qquad (4)$$

where P_o is the total concentration of the RCs in the system (both PSII and PSI), and combining Eq. (4) with Eq.(3) to eliminate P^* and P from the formulation, the following equation is obtained:

$$P^* = IP_o / [(k_d + k_D) / k_e + I] \qquad (5)$$

Since the rate of photosynthetic electron transport is defined as:

$$R_e = k_D P^* \qquad (6)$$

then R_e becomes:

$$R_e = k_D IP_o / [(k_d + k_D) / k_e + I] \qquad (7)$$

Combining the individual rate constants gives:

$$K_I = (k_d + k_D) / k_e \qquad (8)$$

which yields upon substitution:

$$R_e = k_D IP_o / (K_I + I) \qquad (9)$$

* This is why the whole photosynthesis light phase is sometimes considered as an entire photochemical reaction, leading to the formation of the photochemical products, ATP and NADPH.

By introducing the maximum rate of PET:

$$R_m = k_D P_o \tag{10}$$

in Eq. (9), one obtains

$$R_e = R_m I / (K_I + I) \tag{11}$$

Equation (11) expresses the functional relationship between the PET rate, R_e, and the light intensity, I. At low light intensity ($K_I >> I$), the PET rate is nearly proportional to the incident light, I ("light-limited region"). However, at higher I values ($K_I << I$), the rate asymptotically approaches a maximum value, R_m, and is essentially zero-order with respect to the light intensity ("light-saturated system").

When K_I becomes numerically equal to I, the PET rate achieves half of its potential maximum ($K_I = I$, $R_e = R_m/2$). So, the constant K_I can be replaced by i_{50}, the half-saturation light intensity, *i.e.*, half of the intensity necessary to reach the maximal rate of electron-transport. So, Eq. (11) can be rewritten as:

$$R_e = R_m I / (i_{50} + I) \tag{12}$$

or, taken inversely:

$$1/R_e = (i_{50} + I) / R_m I = 1/R_m (i_{50}/I + 1) \tag{13}$$

Finally, R in Eq. (12) can be replaced by qPF (or qPH). The PET rate and fluorescence quenching are undoubtedly two proportional entities: an increase of the PET rate means a decrease of the variable fluorescence level, F_v and, consequently, an increase of qPF. Analogously, R_m can be replaced by q^oPF (or q^oPH), meaning maximal potential conversion into ET intermediates, *i.e.*, maximal energy storage of the absorbed light.

Hence, by substituting the change into Eq.(13), and using I/i_{50} relationship instead of i_{50}/I in the case of PAS data,[33] the following equation results:[33]

$$\begin{aligned} 1/qPF &= 1/ q^oPF (I/i_{50} + 1) \\ 1/qPH &= 1/ q^oPH (I/i_{50} + 1) \end{aligned} \tag{14}$$

The maximal energy storage yield corresponding to the state with all RCs in the open state, has been expressed here in the terms of fluorescence (as q^oPF), and thermal emission (q^oPH). Indeed, the linear relationship between the reciprocals of the two photochemical quenchings and I has been confirmed for a couple of photoinhibition times ($t_{inh.}$), both for fluorescence and thermal emission (Fig. 3a–b). Introduction of the PAS beam of 700 nm did not change anything in the linearity of the plots (not shown). The calculated q^oPF, q^oPH and i_{50} values for the both excitation wavelengths are presented in Table I.

DISCUSSION

There is a clear, at least formal, analogy between the mathematical model describing the kinetic behaviour of the PET chain, derived through Eqs. (2–14), and the Michaelis-Menten kinetic model describing a reaction between a substrate A, and a catalytic en-

zyme E, *via* a potentially reversible transient complex:

$$A + E \underset{k_{-1}}{\overset{k_1}{\rightleftarrows}} [EA] \xrightarrow{k_2} \text{Product} + E \tag{15}$$

The transient complex [EA] corresponds to the transiently excited reaction center, P^* (Eqs. (1–6)). It can undergo back reaction (←, k_{-1} rate constant) leading to the initial reactants, which corresponds to P^* deactivation to its ground state, P (deactivation rate constant, k_d). On the other hand, [EA] may decompose into final products (rate constant k_2), whereby the catalytical enzyme is restored. Just in a formal sense, it corresponds to the decomposition of water: RC does not react with water in a classical chemical reaction, but catalyzes its decomposition *via* the excited state P^*. However, the same steady-state condition can be applied this time on the transient complex concentration ($d[EA]/dt = 0$) – like it was applied on the excited P^* species ($dP^*/dt = 0$) – which yields the same form of the final equation:

$$\upsilon = k_2 E_{tot} A / (k_A + A) \tag{16}$$

as Eq. (9). The reaction rate υ corresponds to the PET rate R_e; the total enzyme concentration, E_{tot}, to the total RCs concentration P_o; the constant K_A to the constant K_I. The I and A analogy will be analyzed in the following text.

The same stands for the reciprocical plots:

$$1/\upsilon = 1/\upsilon_{max} (K_A / A + 1) \tag{17}$$

corresponds to Eq. (13), and its direct derivation, Eq. (14). Hence, the same linear plot, already well known for the $1/\upsilon$ *vs.* $1/A$ dependence (permitting the calculation of υ_{max} and the Michaelis constant, K_A) should be expected for the fluorescence and photoacoustic data. Fig. 3 (a–b) clearly proves its validity. The plots obtained for different photoinhibition times all permit the calculation of the maximal energy storage (expressed as q^oPF for the fluorescence data and as q^oPH for the protoacoustic data) from the intercepts of the plots and of the half-saturation light intensity i_{50} from the intercepts and the slopes. The calculated values are presented in Table I for both the *qPF* and *qPH* data, for the used excitation wavelengths (680 and 700 nm), and for different photoinhibiton times.

Attempts could be made to reveal more of the formal analogy shown above. A long time ago, photosynthesis was divided into two phases, the "light phase", beginning with light absorption and finishing with NADPH and ATP formation (preserving the absorbed light in their chemical bonds), and the "dark phase" consisting of a few cycles of biochemical reactions, but having the NADPH and ATP as the necessary precursors. The division comes not only from the mechanistic point of view (the light initiated phase, and the thermal phase) but also from the kinetic point of view. However, if one looks at the kinetic dimension of the light phase itself (shown together with the redox-position of every participant in the ETC – Fig. 4[34]), it is possible to distinguish ultrafast photophysical processes (light absorption and redistribution among the pigment molecules in the LHC complexes, occuring in the femtosecond time scale; primary separation occuring in reaction traps of

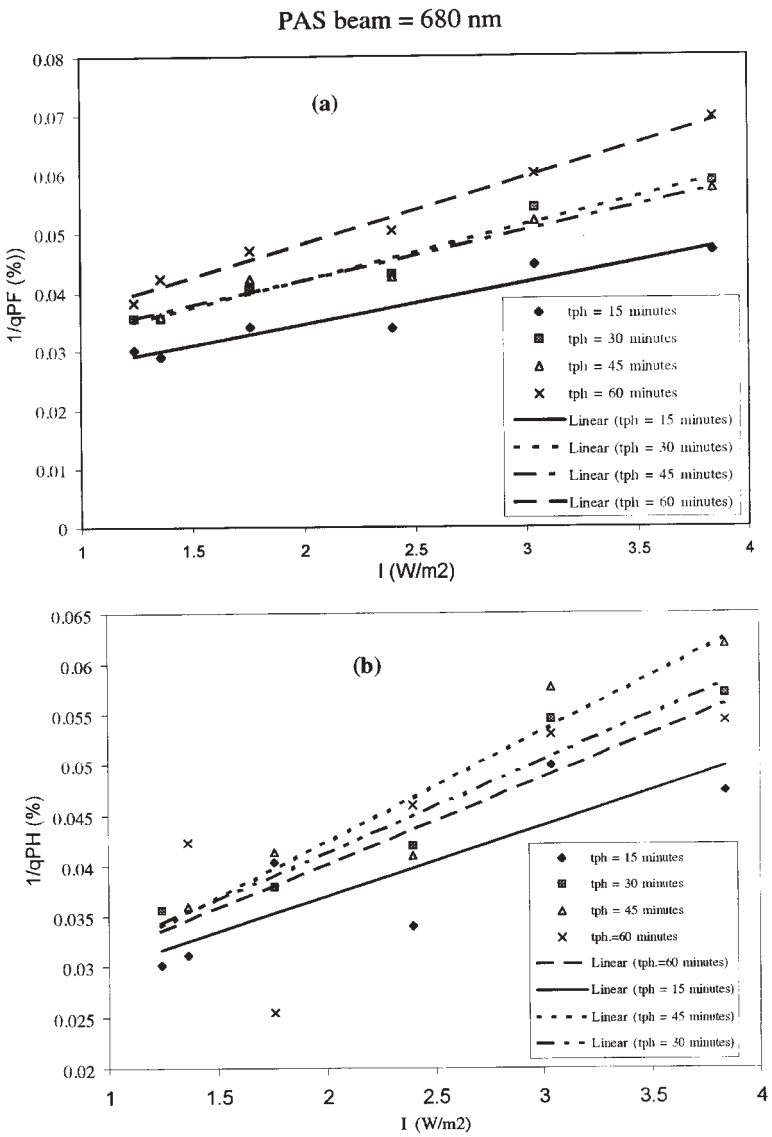

Fig. 3a and b. Reciprocal plots, *i.e.*, 1/*qPF* (upper) and 1/*qPH* (lower) *vs. I*, according to Eq. (14), for isolated thylakoids, photoinhibited for a few periods of time ($t_{ph.}$). λ_{PAS} = 680 nm. *qPF* and *qPH* were calculated from F_m and F_v and H_m and H_v data (like those shown in Fig. 2) as $(F_m - F_v)/F_m$ and $(H_m - H_v)/H_m$, respectively, for the same numbered pulse; then they were averaged since the particular *qPF*(*qPH*) *vs. I* plots almost overlap on the same time scale (not shown). q^oPF and q^oPH, maximal energy storage yield, corresponding to the maximal openness of the reaction centers, has been calculated from the intercept, and the i_{50}, half-saturation light intensity, from the intercept and the slope.

the RCs of the two photosystems and subsequent transfer of the released electrons to the primary acceptors of PSII and PSI, occuring in the picosecond time scale) and the slower

processes, such as decomposition of water, or diffusion controlled reduction of the plastoquinone pool (see Fig. 1), which occur in the millisecond time scale. Hence, it could be said that, whereas the ultrafast events are pure biophysical processes, the other ones, with the indirect or direct participation of proteins (PSII and PSI, as the entities; the ETC components: plastocyanin, cytochromes are metal-protein complexes) are more biochemical in nature. Concretely speaking, the redox state of the primary PSII electron-acceptor Q_A, which directly controls the F_v fluorescent level[34] and so the *qPF* value, is defined by the precedent electron-transfer from pheophytine, and subsequent reduction of Q_B (secondary PSII electron-acceptor), the first one occuring in less than 400 ps, and the latter in 100–600 μs (Fig. 4[34]). Both electron-transfers take place inside the PSII RCs complex, which is clearly protein-embedded (see Fig. 1), and so controlled by the protein composition and geometry. This is a possible connection between Eqs. (14) and (17).

However, if one tries to find a closer connection between the plots represented by Eqs. (14) and (17), *i.e.*, to reveal more of the biochemical background of the plots shown in Fig. 3 (a–b), then one arrives at the question: what is the reactant A (Michaelis-Menten substrate) in these plots (since *I* appears there instead of *A*). The answer comes from the fact that the fluorescence level F_v is directly controlled by the redox state of the quinones (Q) at the acceptor side of the very fluorescent PSII.[35] The quinones, primary acceptors (Q_A) at the PSII acceptor side, are fluorescence quenchers in the oxidized form, while the reduced form (Q_A^-) contributes to the increased fluorescence level.[36] Hence, at lower excitation intensities ("light-limited region"), the oxidized Q_A forms prevail, the PET rate R_e increases and the fluorescence F_v level is very low. However, at higher excitation intensities ("light-saturated regime"), the reduced Q_A^- form dominates causing lower PET rates and leading to the increase of the F_v level. Consequently, *qPF* and *qPH* decrease (Figs. 3a–b). In conclusion, the formal counterpart of the reactant A in Eq. (17) is the primary electron-acceptor Q_A (not appearing in Eq. (14)) – which is why it is the "formal" counterpart – in the oxidized form at lower, and in the reduced form at higher excitation intensities.

The PSII excitation, λ_{P4S} = 680 nm. The *q°PF* and *q°PH* ("maximal energy storage"), which marks the total openness of the reaction centers, generally decrease with increasing length of the photoinhibition time ($t_{ph.}$). However, in the $t_{ph.}$ period of 15–60 min, *q°PF* and *q°PH* slowly decrease (from 42.7 % to 33.3 % in the case of the *qPF* data, and from 39.4 % to 34.7 % in the case of the *qPH* data), and then there is a drop up to $t_{ph.}$ = 100 minutes (19.9 % and 18.9 %, for the *qPF* and *qPH* data, respectively). So, it seems that in $t_{ph.}$ = 15–60 min period, a slow, but continuous inhibition takes place and then there is a serious "hit" occuring in the $t_{ph.}$ = 100 min period. Such a behaviour is partly confirmed by a continuous decrease in i_{50} with increasing $t_{ph.}$ time (with the exception of $t_{ph.}$ = 45 min). Both these facts seem reasonable: it does have a logic that the maximal openness of the reaction centers (expressed either through *q°PF* or *q°PH*), as well as the half intensity (of photoacoustic measuring, the PAS beam) needed to saturate the reaction centers, decrease with increasing $t_{ph.}$ time. Since the FL and PAS experiments were done immediately after photoinhibition, it is maybe premature to assume that the inhibition effects are permanent.

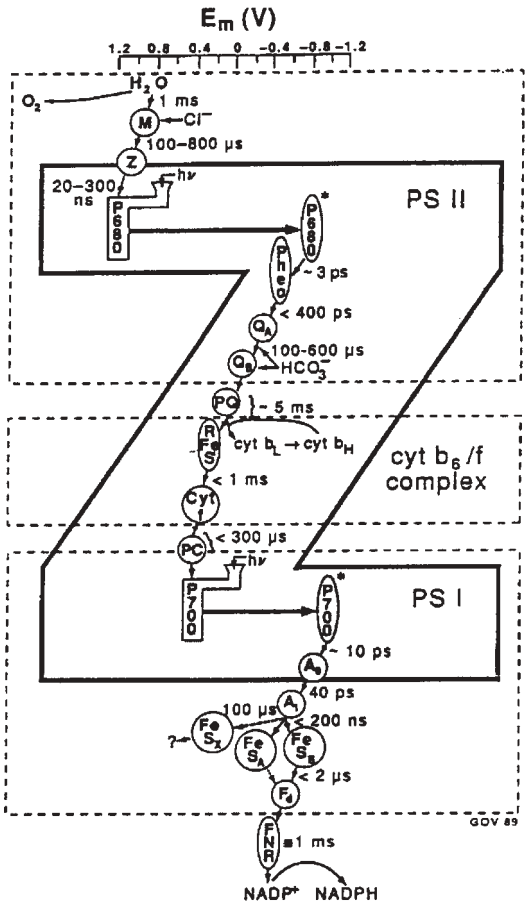

Fig. 4. The Z-scheme of photosynthetic electron transport (PET), with the positions of the participants on the oxido-reduction scale. The time notations of ms, µs, and ps indicate the lifetimes of the respective ET steps. The abbreviations: the same as for Fig. 1. From: Kohen *et al.*: "Photosynthesis" in *Photobiology*, Academic Press, 1995, p. 185.

On the other hand, q^oPF and q^oPH are very close, sometimes almost equal (for $t_{ph.}$ = 30 min q^oPF = 36.8 %, and q^oPH = 36.4 %). Mutual comparison of i_{50} offers a similar conclusion, with the same exception of $t_{ph.}$ = 45 min, the i_{50} from the *qPF* data is 2.8, and from the *qPH* data 2.0 W/m^2).

PSI excitation, λ_{PAS} = 700 nm. The q^oPF and q^oPH, as well as the i_{50} behaviour, are contradictory compared to the λ_{PAS} = 680 nm data. It is difficult to see a persistent behaviour. For example, for $t_{ph.}$ = 30 min, q^oPF = 2.5 % and q^oPH = 53.2 %, and i_{50} from the *qPF* data is 0.4, while from the *qPH* data 3.1 W/m^2. On the other hand, for $t_{ph.}$ = 45 min, $q^oPF = q^oPH$ = 50 %, while i_{50} from the *qPF* data is more than double compared to its *qPH* counterpart (7.1 *vs.* 3.3 W/m^2). This is an inherent impersistent behaviour, when one is aware that these differences do not come from one or two FL and PAS combined experiments. It was necessary to perform six successfull combined FL and PAS experiments after each photoinhibition time (corresponding to six PAS beam intensities values), to create 4 plots (corresponding to the 4 pulses), from which q^oPF and q^oPH and i_{50} were calculated. In addition, for $t_{ph.}$ = 60 and 100 min, the q^oPF and q^oPH values are very close (53.5 % *vs.*

55.9 % for $t_{ph.}$ = 60 min, and 37.0 % *vs.* 35.5 % for $t_{ph.}$ = 100 min), while the i_{50} values are very different (3.7 *vs.* 2.5 W/m^2 for $t_{ph.}$ = 60 min and 5.6 *vs.* 3.4 W/m^2 for $t_{ph.}$ = 100 min). So, with increasing $t_{ph.}$ neither of the two parameters show a clear behaviour. The i_{50} values oscillate and it is difficult to determine where the "maximum" is and where the "minimum" is. The q^oPF and q^oPH values both drop to 37.0 and 35.5 % for $t_{ph.}$ = 100 min, after the two 50 % values for the previous $t_{ph.}$ periods (45 and 60 min).

Generally, λ_{PAS} = 700 nm produced higher plot values for both the q^oPF and q^oPH data, then λ_{PAS} = 680 nm (Table I). It is almost the same for i_{50} (Table I). Hence, PSI is ready to receive more photons, and generally needs more light to obtain saturation after the photoinhibition pretreatment. Clearly, PSI appears to be less affected than PSII.

TABLE I. The q^oPF and q^oPH, maximal energy storage yield, corresponding to the maximal openness of the reaction centers, and the i_{50}, half-saturation light intensity, calculated from the plots shown in Figs. 3a and b, for a couple of photoinhibition periods, λ_{PAS} = 680 nm data (left), λ_{PAS} = 700 nm data (right).

Time of photoinhibition/min	λ_{PAS} =680 nm				λ_{PAS} = 700			
	qPF		*qPH*		*qPF*		*qPH*	
	q^oPF/ %	i_{50}/Wm^{-2}	q^oPH/ %	i_{50}/Wm^{-2}	q^oPF/ %	i_{50}/Wm^{-2}	q^oPH/ %	i_{50}/Wm^{-2}
15	42.7	3.16	39.4	3.23	–	–	–	–
30	36.8	2.7	36.4	2.9	2.5	0.4	53.2	3.1
45	33.1	2.8	37.0	2.0	50.0	7.1	50.0	3.3
60	33.3	2.5	34.7	2.8	53.5	3.7	55.9	2.5
100	19.9	2.3	18.9	2.3	37.0	5.6	35.5	3.4

Acknowledgements: The author thanks the National Research Council of Canada for granting him a one-year postdoctoral fellowship at Université du Québec, which provided the experimental data for this manuscript.

ИЗВОД

СКЛАДИШТЕЊЕ ЕНЕРГИЈЕ У ФОТОСИНТЕТСКОМ ЕЛЕКТРОН-ТРАНСПОРТНОМ ЛАНЦУ. АНАЛОГИЈА СА МИХАЕЛИС-МЕНТЕНОВОМ КИНЕТИКОМ

ДЕЈАН МАРКОВИЋ

Технолошки факултет, 16000 Лесковац

Применом комбиноване флуоресцентне и фотоакустичне технике у раду је извршено истовремено мерење флуоресценције и термалне емисије из изолованих тилакоидних мембрана претходно изложених продуженом дејству засићујуће светлости. Из добијених сигнала конструисани су Лајнвивер-Баркови типови графика доказујући барем формалну аналогију између кинетике механизама флуоресценције и термалне емисије из изолованих тилакоидних мембрана, и Михаелис-Ментенове кинетике за ензимске реакције. Из ових графика израчуната су два карактеристична параметра (складиштена енергија и полузасићујући светлосни интензитет) у циљу добијања основног, почетног одговора о функционисању фотосинтетског апарата под условима фотоинхибирајућег стреса.

(Примљено 28. августа 2002)

REFERENCES

1. W. H. He, R. Malkin, *Photosynthesis*, Cambridge University Press, 1998, p. 29
2. K. Sauer, *Encyclopedia of Plant Physiology*. New Series. Photosynthesis III, Vol. 19, Springer-Verlag, 1986, p. 85
3. Govindjee, in *Probing Photosynthesis. Mechanisms, Regulation and Adaptation*, M. Younis, U. Pathre, P. Mohanty, Eds., Taylor and Francis, 2000, p. 9
4. R. Singh, in *Probing Photosynthesis. Mechanisms, Regulation and Adaptation*, M. Younis, U. Pathre, P. Mohanty, Eds., Taylor and Francis, 2000, p. 169
5. J. M. Howel, W. R. Vieth, *J. Mol. Catalysis* **16** (1982) 245
6. B. Ke, *Photosynthesis; Photobiochemistry and Photobiophysics*, *Advances in Phtosynthesis*, Vol. 10, Kluwer Academic Publishers (2001), p. 321
7. W. L. Butler, *Encyclopedia of Plant Physiology*, New Series 5, Springer-Verlag, 1977, p. 149
8. S. Malkin, D. Cahen, *Phtochem. Photobiol.* **29** (1979) 803
9. N. Lasser-Ross, S. Malkin, D. Cahen, *Biochim. Biophys. Acta* **593** (1980) 330
10. R. Carpentier, R. M. Leblanc, M. Mimeault, *Enzyme Microb. Technol.* **9** (1987) 489
11. R. Carpentier, H. Y. Nakatani, R. M. Leblanc, *Biochim. Biophys. Acta* **808** (1985) 470
12. R. Carpentier, B. LaRue, R. M. Leblanc, *Arch. Biochem. Biophys.* **228** (1984) 534
13. A. Yamagishi, S. Katoh, *Biochim. Biophys. Acta* **766** (1984) 215
14. O. Canaani, *Biochim. Biophys. Acta* **852** (1986) 74
15. G. Bults, B. A. Horwitz, S. Malkin, D. Cahen, *Biochim. Biophys. Acta* **679** (1982) 452
16. C. Buschmann, K. Prehn, *Photobiochem. Photobiophys.* **5** (1983) 63
17. M. Havaux, *Env. Exp. Bot.* **30** (1990) 101
18. G. Ouzounidou, R. Lannoye, S. Karataglis, *Plant Science* **89** (1993) 221
19. M. Havaux, F. Tardy, *Planta* **198** (1996) 324
20. M. Havaux, F. Tardy, *J. Photochem. Photobiol., B:Biol.* **40** (1997) 68
21. R. Carpentier, T. G. Owens, R. M. Leblanc, *Photochem. Photobiol.* **53** (1991) 565
22. M. Velitchkova, R. Carpentier, *Photosynth. Res.* **40** (1994) 263
23. C. Buschmann, *Photosynt. Res.* **14** (1987) 229
24. C. Buschmann, L. Kocsanyi, *Photosynth. Res.* **21** (1989) 129
25. J. F. H. Snel, M. Kooijman, W. J. Vredenberg, *Photosynth. Res.* **25** (1990) 259
26. D. Z. Marković, R. Carpentier, *Biochem. Cell Biol.* **73** (1995) 247
27. W. Yahyaoui, D. Marković, R. Carpentier, *Optical Engineering* **36** (1997) 337
28. S. I. Allakhverdiev, V. V. Klimov, R. Carpentier, *Proc. Natl. Acad. Sci. USA* **91** (1994) 281
29. V. B. Curwiel, J. J. S. van Rensen, *Physiol. Plantarum* **89** (1993) 97
30. B. Genty, J-M. Briantais, N. R. Baker, *Biochim. Biophys. Acta* **990** (1989) 87
31. B. Genty, J. Harbinson, J-M. Briantais, N. R. Baker, *Photosynth. Res.* **25** (1990) 249
32. O. van Kooten, J. F. H. Snel, *Photosynth. Res.* **25** (1990) 147
33. R. Carpentier, R. M. Leblanc, M. Mimeault, *Biochim. Biophys. Acta* **975** (1989) 370
34. E. Kohen, R. Santus, J. H. Hirschberg, *Photobiology*, Academic Press, 1995, p. 177
35. U. Schreiber, W. Bilger, H. Hormann, C. Heubauer, *Photosynthesis*, Cambridge University Press, 1998, p. 320
36. K. Karukstis, *Chlorophylls*, CRC Press, 1991, p. 769.